PRAMANA
— journal of
physics

Vol. 65, No. 4
October 2005
pp. 713–722

Nanostructured copper particles-incorporated Nafion-modified electrode for oxygen reduction

T SELVARAJU and R RAMARAJ*
Centre for Photoelectrochemistry, School of Chemistry, Madurai Kamaraj University, Madurai 625 021, India
Corresponding author. E-mail: ramarajr@yahoo.com

Abstract. The electrocatalytic activity of nanostructured copper particles (represented as Cu_{nano}) incorporated Nafion (Nf) film-coated glassy carbon (GC) electrode ($GC/Nf/Cu_{nano}$) towards oxygen reduction was investigated in oxygenated 0.1 M phosphate buffer (pH 7.2). The electrodeposited Cu_{nano} in Nf film was characterized by atomic force microscopy (AFM) and X-ray photoelectron spectroscopy (XPS). The electrocatalytic activity of Cu_{nano} at the modified electrode towards oxygen reduction was studied using cyclic voltammetry technique. The molecular oxygen reduction at the $GC/Nf/Cu_{nano}$-modified electrode started at a more positive potential than at a bare GC electrode. A possible reaction mechanism was proposed in which oxygen reduction may proceed through two-step two-electron processes at the $GC/Nf/Cu_{nano}$ electrode. The $GC/Nf/Cu_{nano}$ electrode shows higher stability for oxygen reduction in neutral solution and the electrode may find applications in fuel cells.

Keywords. Nafion; copper nanoparticles; modified electrode; oxygen reduction; catalysis.

PACS Nos 81.07.Bc; 82.35.Np; 82.45.Jn; 82.45.-h

1. Introduction

Oxygen reduction reaction is very important in many processes, such as electrochemical energy conversion/storage, metal corrosion, fuel cell and electrocatalysis [1–5]. Different materials have been proposed as electrocatalysts for oxygen reduction and the mechanism of electrochemical reduction of molecular oxygen at such electrode materials has been extensively studied [1–5]. Hydrogen peroxide is an unwanted side product that reduces the power conversion efficiency. The kinetics of oxygen reduction have been extensively investigated at catalysts-incorporated modified electrodes [5–8]. Various organic and inorganic modifiers have been immobilized on the electrode surface to prepare chemically modified electrodes (CMEs) [9]. The deliberate modification of the solid phase component of an electrode/solution interface provides better electrode materials that differ from those of the bare electrode. Uosaki and co-workers [5] studied the electrochemical reduction of oxygen at the ultra-thin palladium layers of various thickness on Au(111) and Au(100)

single crystal surfaces in 50 mM $HClO_4$ solution saturated with oxygen. Our group has studied the electrochemical reduction of oxygen at platinum microparticles deposited modified electrodes in acidic medium [7]. On the other hand, its reduction in neutral solution is interesting in the development of biosensors for dissolved oxygen in biological samples [10–12]. Metal microparticles deposited on electrode surface with and without polymer coatings and their resulting electrocatalytic properties have been reported [13–15]. Polymer films, such as Nafion, enhance the stability and dispersity of the embedded platinum microparticles on electrode surfaces [7]. The high organization of metal nanoparticles on the electrode surface provides cooperative and homogeneous behavior for the entire electrode surface. The metal nanocolloids that are immobilized on solid supports are found to be attractive precursors for chemical and electrochemical catalysis [16]. Only few groups have reported the electrocatalytic reactions at metal nanoparticles-modified glassy carbon electrode [16]. Recently, we have reported the biosensor applications of platinum and copper nanoparticles-modified electrodes [17,18]. In the present communication, the electrodeposition of nanostructured copper particles (represented as Cu_{nano}) onto Nf film-coated GC electrode and their electrocatalytic properties towards oxygen reduction are reported.

2. Experimental

2.1 *Reagents*

Copper sulphate, sodium perchlorate, mono-sodium and di-sodium hydrogen phosphate (Merck) were used as received. Pure grade oxygen gas was used for saturating the solutions. Unless otherwise noted, a 0.1 M phosphate buffer solution (PBS, pH 7.2) was used for all the electrochemical measurements.

2.2 *Electrochemical measurements*

The electrochemical experiments were performed with an EG&G PAR model 283 potentiostat/galvanostat controlled by Echem software. The electrochemical measurements were carried out using a three-electrode system with a Cu_{nano}-modified GC electrode (area = 0.07 cm^2) as working electrode, platinum wire as counter electrode and standard calomel electrode (SCE) as reference electrode.

2.3 *Preparation and surface characterization of nanostructured copper particles-modified glassy carbon electrode*

Nanostructured copper particles were deposited electrochemically on GC electrode using a deaerated solution of 0.01 M $CuSO_4$ and 0.1 M $NaClO_4$ under different applied potentials (E_{app} = 0.0–0.6 V (SCE)). Better electrocatalytic activity could be achieved when Cu_{nano} was electrodeposited at −0.4 V at a charge of 700 μC. Prior to every experiment, the electrodes were polished with an aqueous suspension

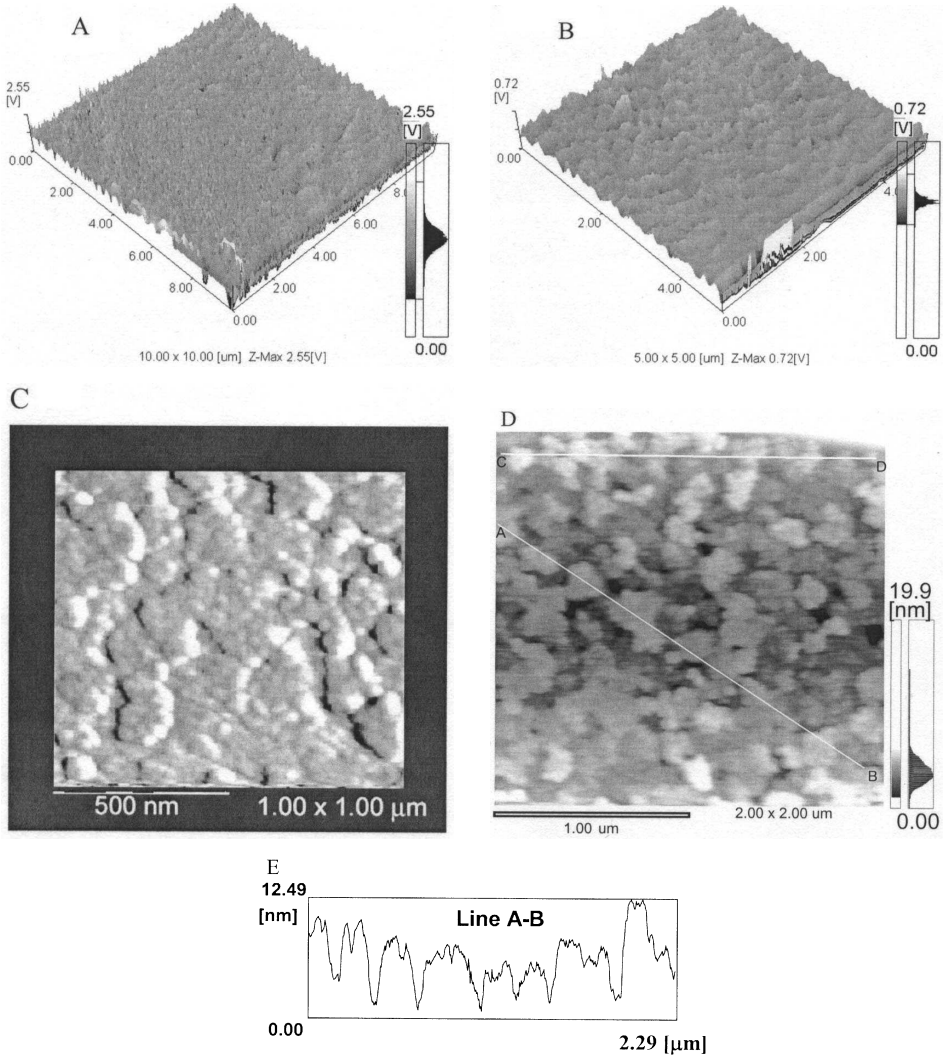

Figure 1. Tapping mode of 3D AFM images of ITO/Nf (**A**) and ITO/Nf/Cu_{nano} (**B**) electrode surfaces. Cu_{nano} was deposited at an applied potential of −0.4 V (SCE) (Nf film thickness = 0.9 μm). (**C**) 2D AFM image (1.0 μm × 1.0 μm) of ITO/Nf/Cu_{nano} electrode, (**D**) 2D AFM image (2.0 μm × 2.0 μm) of ITO/Nf/Cu_{nano} electrode and (**E**) cursor plot for the line AB shown in figure 1D.

of 1.0 μm and 0.05 μm alumina on a Buehler cloth, rinsed copiously with doubly distilled water and sonicated in a water bath for 3 min followed by activation to remove the charging currents. The AFM images of the copper nanoparticles incorporated into Nafion film were measured using Shimadzu SPM 9500 scanning probe microscope and XPS was recorded using Perkin-Elmer 5600 X-ray photoelectron

spectrometer equipped with a EA 10/100 multichannel detector (Specs). MgK_α radiation (1253.6 eV, 12 kV) with full-width at half-maximum (0.7 eV) was used for the excitation.

3. Results and discussion

3.1 *Characterization of nanostructured copper particles-incorporated Nafion film-modified electrode (GC/Nf/Cu)*$_{\text{nano}}$

The surface morphology of Cu nanoparticles electrodeposited on indium tin oxide (ITO) electrode was examined by atomic force microscopy (AFM). Figure 1A shows the AFM images of the Nafion polymer coated on ITO electrode (ITO/Nf). The AFM images of Cu nanoparticles-incorporated Nafion-coated ITO electrode (ITO/Nf/Cu_{nano}) surface is shown in figure 1B. The morphology of Cu nanoparticles on ITO substrate shows faceted grains indicating that the Cu particles in the film are well-crystallized and display a preferred orientation. The morphology shown in figure 1B is clearly different from that of figure 1A. The 2D AFM image of the ITO/Nf/Cu_{nano} (figure 1C) shows the aggregated smaller Cu_{nano} particles. Figure 1D shows the larger aggregates of Cu_{nano} on ITO/Nf electrode. The sizes of the aggregates are measured from the cursor plot shown in figure 1E (obtained for line AB shown in figure 1D) varies from 20 to 200 nm. This observation shows that the electrodeposition of Cu_{nano} leads to the formation of nanostructured Cu particles with smaller grains in the range 15–25 nm and the larger aggregates in the range 130–200 $\pm$10 nm.

XPS was used to investigate the valence of Cu_{nano} particles electrodeposited onto the ITO/Nf electrode and figure 2 shows the XPS obtained for the Cu nanoparticles in Nf film. Due to the presence of excess stabilizer, which leads to carbon/metal ratios of >70, long data acquisition times are necessary. The emission of 2p photoelectrons from Cu is identified in two peaks of the XPS spectra, one is assigned to Cu(0) (935 eV) and the other one to Cu(I) (955 eV). XPS measurements lead to confirm the complete reduction of $CuSO_4$ and the formation of Cu(0) on Nafion-coated ITO. It is necessary to point out that in many instances, the layered nature of the film is obscured by interpenetration of the subsequent layers and high interlayer roughness and by embedding of particles on the polymer film. In the case of Cu, binding energy and FWHM (full-width at half-maximum) data can be unambiguously derived from the respective signals. The observed Cu(2p) binding energies indicate the presence of Cu(0) and Cu(I) (Cu_2O) species. This means that during electrodeposition, Cu exist in the +0 and +1 oxidation states. The peak with binding energy of 935 eV is assigned to the presence of Cu metal [19]. The peak at 955 eV is more difficult to assign because bulk cuprous oxides have similar binding energies [19].

3.2 *Cyclic voltammetric studies of nanostructured copper particles-modified electrode*

Figure 3 shows the cyclic voltammograms recorded for oxygen reduction at bare GC electrode (figure 3a) and after Cu nanoparticles incorporated into Nf

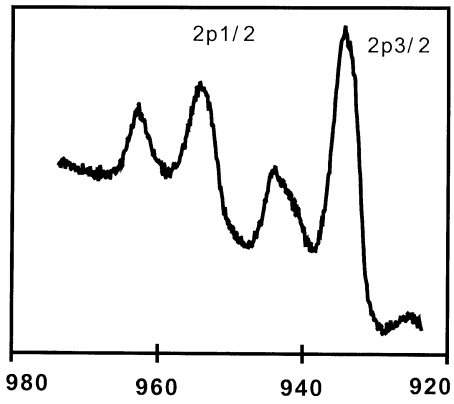

Figure 2. High-resolution XPS of $Cu(2p_{3/2-1/2})$ core-level spectra of electrodeposited Cu on ITO/Nf electrode ($ITO/Nf/Cu_{nano}$).

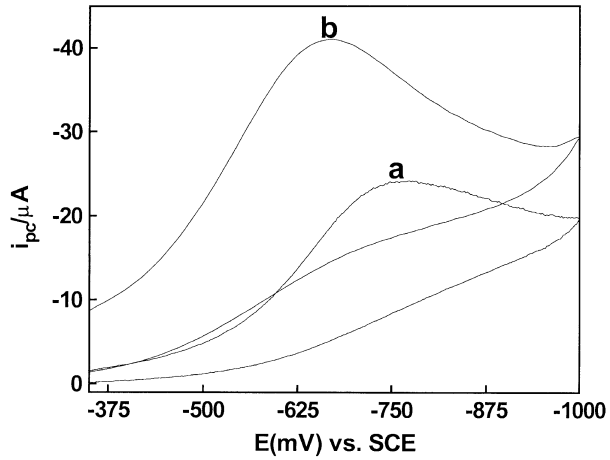

Figure 3. Cyclic voltammograms recorded for oxygen reduction at bare GC electrode (**a**) and $GC/Nf/Cu_{nano}$ electrode (**b**) in oxygen saturated 0.1 M PBS. Cu_{nano} was deposited at an applied potential of −0.4 V (SCE).

film-coated GC electrode (figure 3b) in oxygen saturated 0.1 M PBS. Under deaerated condition, the GC electrode did not show any reduction peak in the potential region −1.0 to −0.35 V. When the solution was saturated with oxygen, a reduction peak was observed in the cyclic voltammogram as shown in figure 3. The oxygen reduction peak was observed at −0.76 V at bare GC electrode in 0.1 M PBS. At $GC/Nf/Cu_{nano}$ electrode oxygen reduction occurs at −0.63 V with an increase in the reduction peak current and a decrease in overpotential when compared to bare GC electrode. This result suggests that the $GC/Nf/Cu_{nano}$ electrode can be used for catalytic oxygen reduction in neutral solution.

Different forms of Cu_{nano} were deposited on GC electrode at different applied potentials (E_{app}) by electrodeposition and used for oxygen reduction. Figure 4

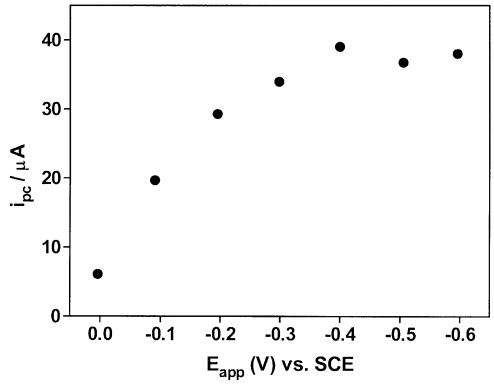

Figure 4. Effect of different applied potentials on the formation of Cu_{nano} particles onto Nf-coated GC electrode ($GC/Nf/Cu_{nano}$). The O_2 reduction peak current in 0.1 M PBS is taken as the measure of Cu_{nano} formation at different applied potentials (total applied charge = 0.011 C/cm^2).

shows the effect of applied potentials on the oxygen reduction peak currents for $GC/Nf/Cu_{nano}$ electrodes prepared at different applied potentials ($E_{app} = 0$, -0.1, -0.2, -0.3, -0.4, -0.5 and -0.6 V (SCE)). The oxygen reduction peak current increased at more negative potentials and reached a maximum at -0.4 V. The difference in the electrochemical behavior of the Cu_{nano}-modified electrode is due to the partially charged copper (Cu^0 and Cu^+) monolayer formed around 0 to -0.2 V with co-adsorbed perchlorate anion to attain electrical neutrality, which is close to the stripping potential of metallic copper. The partially charged copper nanostructures (Cu^0 and Cu^+) initially deposited with co-adsorbed perchlorate anions attributes to the poor performance for oxygen reduction at $GC/Nf/Cu_{nano}$ electrode. The metallic copper nanoparticles deposited at -0.4 V result in the complete desorption of perchlorate anions from the Cu_{nano} film at the modified electrode and leads to the formation of multilayer copper nanostructures on the electrode surface. The Cu_{nano}-modified electrode prepared at -0.4 V showed better electrocatalytic behavior towards oxygen reduction.

Figure 5 shows the plot of the effect of charge consumed during Cu_{nano} electrodeposition at -0.4 V ($GC/Nf/Cu_{nano}$) on the oxygen reduction peak current. The peak current increased as the charge consumed for Cu_{nano} deposition increased and attained saturation around 0.011 C/cm^2 for the $GC/Nf/Cu_{nano}$ electrode. Figure 6 shows the cyclic voltammograms recorded for oxygen reduction at Cu_{nano} deposited on GC (figure 6a) and GC/Nf electrodes (figure 6b). An observable difference in the peak currents was not noticed. However, the oxygen reduction peak potential shifted to more positive at $GC/Nf/Cu_{nano}$ electrode. Figure 6 shows the activity of Cu_{nano} towards oxygen reduction in the absence and presence of Nafion film on the GC electrode. The decrease in the overpotential observed for oxygen reduction in Figure 6b ($GC/Nf/Cu_{nano}$) when compared to figure 6a (GC/Cu_{nano}) shows that the highly acidic Nafion film favors the proton involved oxygen reduction reaction (eqs (2) and (3)) at the Cu_{nano}-incorporated Nafion film-modified electrode. Figure 7 shows the plot of peak current against the square root of scan rate observed for

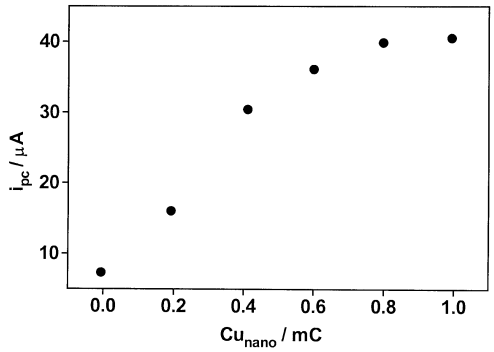

Figure 5. Electrocatalytic reduction of O_2 at GC/Nf/Cu_{nano} electrode in oxygen-saturated 0.1 M PBS. Effect of different amounts of charge consumed during electrodeposition of Cu_{nano} particles onto Nf-coated GC electrode on the oxygen reduction reaction. The O_2 reduction peak current is taken as the measure of different amount of charge consumed at $E_{app} = -0.4$ V (GC electrode area = 0.07 cm^2).

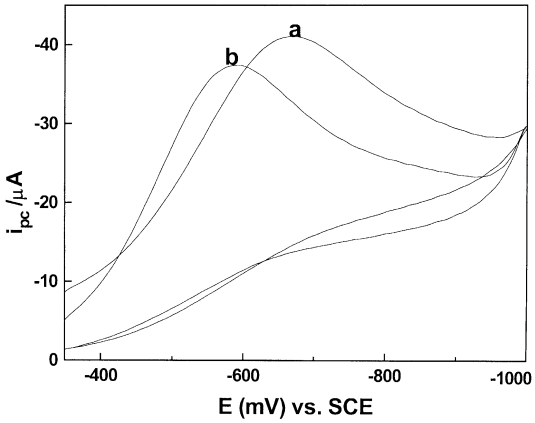

Figure 6. Cyclic voltammograms recorded at (**a**) GC/Cu_{nano} and (**b**) GC/Nf/Cu_{nano} electrodes in oxygen-saturated 0.1 M PBS. Cu_{nano} was deposited at an applied potential of −0.4 V (SCE).

oxygen reduction at GC/Nf/Cu_{nano} electrode. The observed linear plot (figure 7) indicates that the oxygen reduction at GC/Nf/Cu_{nano} electrode follows diffusion-controlled process. This means that the Faradaic current (i_p) whose magnitude is controlled by the rate at which a reactant in an electrochemical process diffuses toward an electrode–solution interface (and, sometimes, by the rate at which a product diffuses away from that interface) is controlled by diffusion of the analytes (eq. (1)).

$$i_p = (2.69 \times 10^5) n^{3/2} A D^{1/2} \upsilon^{1/2} C_0, \tag{1}$$

where n, A, D, C_0 and υ represent the number of electrons, working electrode

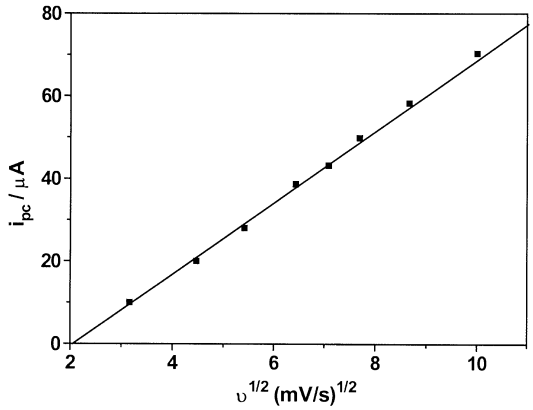

Figure 7. Plot of electrocatalytic oxygen reduction peak current (i_{pc}) as a function of square root of scan rate observed for oxygen reduction at GC/Nf/Cu_{nano} electrode in oxygen-saturated 0.1 M PBS. Cu_{nano} was deposited at an applied potential of −0.4 V (SCE).

area, diffusion coefficient of the species, concentration of reactant and scan rate, respectively.

It should be noted that the cathodic peak current observed during oxygen reduction includes the current due to the reduction of cuprous oxide (Cu_2O), if any, to Cu(0). It is impossible to separate these two contributions accurately. However, the cathodic limiting currents observed during oxygen reduction at the GC/Nf/Cu_{nano} electrode were much larger than that of the peak currents observed for the cuprous oxide reduction, which was confirmed from the cathodic peak currents observed in the deaerated solution. Thus, it is reasonable to conclude that the major contribution to the peak current comes from the catalytic oxygen reduction reaction at GC/Nf/Cu_{nano} electrode. A two-step process can explain the possible oxygen reduction mechanism at the modified electrode. As proposed by Yeager [20], the oxygen reduction in aqueous solution generally proceeds by either of the two pathways (Scheme 1).

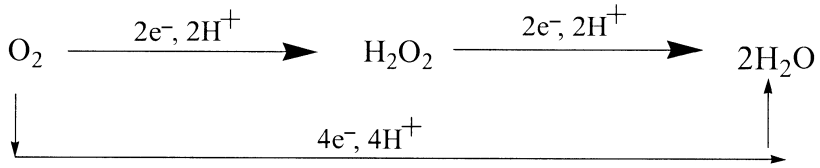

Scheme 1. Oxygen reduction to H_2O by two pathways.

One pathway is the direct four-electron reduction of oxygen to water. The other pathway is through the two-electron reduction leading to H_2O_2 intermediate followed by further reduction to water. At the GC/Nf/Cu_{nano} electrode, it is assumed that the two-electron reduction process leads to the formation of H_2O_2 intermediate in which the intermediate could not be trapped due to faster electrode kinetics and reactions (2) and (3) take place consecutively.

$$O_2 + 2e^- + 2H^+ \rightarrow H_2O_2, \tag{2}$$

$$H_2O_2 + 2e^- + 2H^+ \rightarrow 2H_2O. \tag{3}$$

Practically no decrease in the oxygen reduction current was observed for the GC/Nf/Cu_{nano} electrode under continuous bubbling of oxygen in the PBS solution. This shows that the modified electrode is stable towards the electrocatalytic oxygen reduction.

4. Summary

Cu nanoparticles were electrodeposited onto Nf film-coated electrode. The Cu_{nano} particles deposited in the Nf film were characterized by AFM and XPS. The electrocatalytic activity of GC/Nf/Cu_{nano} electrode towards oxygen reduction in neutral solution was demonstrated through cyclic voltammetry studies. When compared to bare GC electrode and GC/Cu_{nano} electrodes, GC/Nf/Cu_{nano} electrode showed better electrocatalytic activity and stability for oxygen reduction. Cyclic voltammetric studies at different scan rates showed that the oxygen reduction process at GC/Nf/Cu_{nano} electrode was diffusion-controlled. The possible reaction mechanism for oxygen reduction at GC/Nf/Cu_{nano} electrode was proposed (eqs (2) and (3)). The reduction of oxygen in neutral medium at the GC/Nf/Cu_{nano}-modified electrode may proceed through a two-step two-electron process. The role of Nf film on the catalytic oxygen reduction reaction at the modified electrode is two-fold: (i) The Nf membrane is known to concentrate molecular oxygen in the swelled ionic cluster regions of the membrane [21] and (ii) the highly acidic Nf membrane [22] will favor the proton coupled oxygen reduction reaction. The highly dispersed Cu nanoparticles with high surface area in Nf film suggests that the Cu_{nano}-modified electrode may find potential applications in many other electrocatalytic reactions including electrochemical sensor applications. Further work is in progress to study the electrode reaction kinetics.

Acknowledgement

We acknowledge the financial support from the Department of Science and Technology, New Delhi and CSIR for the fellowship to TS.

References

[1] V S Murthi, R C Urian and S Mukerjee, *J. Phys. Chem.* **B108**, 11011 (2004)
[2] B Sljukic, C E Banks and R G Compton, *Phys. Chem. Chem. Phys.* **6**, 4034 (2004)
[3] I Yagi, T Ishida and K Uosaki, *Electrochem. Commun.* **6**, 773 (2004)
[4] V Soukharev, N Mano and A Heller, *J. Am. Chem. Soc.* **126**, 8368 (2004)
[5] H Naohara, S Ye and K Uosaki, *Electrochim. Acta* **45**, 3305 (2000)
[6] V Ganesan and R Ramaraj, *J. Appl. Electrochem.* **30**, 757 (2000) and references cited there in

[7] J Premkumar and R Ramaraj, *J. Solid State Electrochem.* **1**, 172 (1997)
[8] K V Gobi and R Ramaraj, *J. Electroanal. Chem.* **449**, 81 (1998)
[9] R W Murray (ed.), *Molecular design of electrode surfaces* (J. Wiley & Sons, New York, 1992)
[10] P Delahay, *J. Electroanal. Chem.* **97**, 198 (1950)
[11] E S Brandt, *J. Electroanal. Chem.* **150**, 97 (1983)
[12] P Gouerec, A Bilou, O Contamin, G Scarbeck, M Savy, J M Barbe and R Guilard, *J. Electroanal. Chem.* **398**, 67 (1995)
[13] I Rubinstein and A J Bard, *J. Am. Chem. Soc.* **102**, 6641 (1980)
[14] S Duron, R Rivera-Noriega, P Nkeng, G Poillerat and O Solorza-Feria, *J. Electroanal. Chem.* **566**, 281 (2004)
[15] M S El-Deab and T Ohsaka, *J. Electroanal. Chem.* **553**, 107 (2003)
[16] K M Kost, D E Bartak, B Kazee and T Kuwana, *Anal. Chem.* **62**, 1 (1990)
[17] T Selvaraju and R Ramaraj, *J. Electroanal. Chem.* (in press)
[18] T Selvaraju and R Ramaraj, to be published
[19] D K Sarkar, X J Zhou, A Tannous and K T Leung, *J. Phys. Chem.* **B107**, 2879 (2003)
[20] E Yeager, *J. Mol. Catal.* **38**, 5 (1986)
[21] Z Ogumi, T Kuroe and Z Takehara, *J. Electrochem. Soc.* **132**, 1095 (1985)
[22] J P Hwang, G K Suryaprakash and G A Olah, *Tetrahedron* **56**, 7199 (2000)